ELSEVIER

Journal of Luminescence 99 (2002) 149–154

JOURNAL OF LUMINESCENCE

www.elsevier.com/locate/jlumin

Temperature dependence of excitonic luminescence from nanocrystalline ZnO films

X.T. Zhang*, Y.C. Liu, Z.Z. Zhi, J.Y. Zhang, Y.M. Lu, D.Z. Shen, W. Xu, X.W. Fan, X.G. Kong

Open Laboratory of Excited State Processes, Chinese Academy of Science, Changchun Institute of Optics, Fine Mechanics and Physics, 1-Yan An Road, Changchun 130021, People's Republic of China

Received 20 August 2001; received in revised form 28 January 2002; accepted 1 March 2002

Abstract

The properties of the excitonic luminescence for nanocrystalline ZnO thin films are investigated by using the dependence of excitonic photoluminescence (PL) spectra on temperature. The ZnO thin films are prepared by thermal oxidation of ZnS films prepared by low-pressure metalorganic chemical vapor deposition (LP-MOCVD) technique. The X-ray diffraction (XRD) indicates that ZnO thin films have a polycrystalline hexagonal wurtzite structure with a preferred (0 0 2) orientation. A strong ultraviolet (UV) emission peak at 3.26 eV is observed, while the deep-level emission band is barely observable at room temperature. The strength of the exciton–longitudinal-optical (LO) phonon coupling is deduced from the temperature dependence of the full-width at half-maximum (FWHM) of the fundamental excitonic peak, decrease in exciton–longitudinal-optical (LO) phonon coupling strength is due to the quantum confinement effect.

PACS: 78.55.Et; 81.05.Dz; 81.15.Gh; 78.30.Fs; 81.05.Ys

Keywords: Excitonic luminescence; Photoluminescence; Thermal oxidation; LP-MOCVD; Nanocrystalline ZnO thin film

1. Introduction

As a wide band gap ($E_g = 3.37$ eV) semiconductor, ZnO has attracted considerable attention due to its potential applications, such as ultraviolet light-emitting devices and laser devices. Compared with other wide band gap materials, ZnO has a larger exciton binding energy (59 meV) [1], which assures more efficient exciton emissions at higher temperatures. A notable discovery in ZnO thin film materials is the observation of the ultraviolet (UV) stimulated emission induced by the exciton–exciton scattering at moderate pumping intensity [2–4]. These results show that the ZnO is a suitable candidate for optoelectronic device applications in the ultraviolet region. To obtain an efficient and stable UV exciton emission from ZnO films, it is necessary to know the energy band structure of ZnO. The three valence bands of wurtzite semiconductors are nondegenerate and result in the excitons, labeled A, B and C. In the case of ZnO, it should be noted that the valence band structure differs from that of other wurtzites because of the

*Corresponding author.
E-mail address: xitianzhang@163.com (X.T. Zhang).

0022-2313/02/$ - see front matter
PII: S0022-2313(02)00331-9

negative spin-orbit coupling. The ordering of valence bands is Γ_7, Γ_9 and Γ_7, while the conduction band has Γ_7 symmetry [5]. This imposes selection rules for optical transitions, so the A- and B-excitons have large oscillator strength for $E \perp c$ (c represents a crystal axis) polarization and $E//c$ polarization is necessary for the C-exciton. It is difficult to distinguish these peaks in ZnO films because these excitons have approximate energies and large nonradiative damping constants. Recently, room temperature stimulated emissions have been experimentally confirmed [2–4]. UV stimulated emission is attributed to the exciton–exciton scattering at moderated excitation intensity. For these reasons, it is necessary to study the excitonic emissions of nanometer ZnO films in details. Few studies have been done in this area [6,7]. In this paper, the dependence of the exciton emissions in nanocrystalline ZnO films on temperature is studied, where the ZnO films are prepared by thermal oxidation of ZnS films prepared on quartz subtracts using the low-temperature metalorganic chemical vapor deposition (LP-MOCVD) technique. The origin of the luminescence will be discussed with the help of PL spectra.

2. Experiment

The ZnO films used in this study were prepared by thermal oxidation of ZnS films. The ZnS thin films were grown on quartz substrates using dimethyl zinc (DMZn) and hydrogen sulfide (H_2S) by LP-MOCVD. The flow rates of DMZn and H_2S were fixed at 28.65×10^{-6} mol/min and 4.00×10^{-4} mol/min, respectively. Hydrogen (H_2) was used as the carrier gas to transport the reactant, and the total flow rate was kept at 1.3 LMP/min. The pressure of the growth chamber was 300 Torr. In order to remove impurities on the surface, the substrates were pretreated at 600°C for 10 min. The films were deposited on quartz substrates which were maintained at 320°C. The thickness of the deposited ZnS thin films was about 1.5 μm. After deposition, the films were removed from the deposition chamber and placed in a thermal oxidation furnace. Thermal oxidation of the films was carried out in oxygen ambient at 800°C for 2 h. In order to characterize the crystal structure of these films, X-ray diffraction (XRD) spectra were measured using a D/max-rA X-ray diffraction spectrometer (Rigaku) with a Cu K_α line of 1.54 Å. In order to study the luminescent properties of the films, the samples were excited by a He–Cd laser with a wavelength of 325 nm, and with a power of 50 mW. The laser beam was focused to a spot of 30 μm. The monochromator used for the PL measurements has a grating of 600 groove/mm with a blaze wavelength of 400 nm. The luminescence signals were acquired by an UV Microlaser Raman spectrometer made in France.

3. Results and discussion

The ZnO film structure is examined by $\theta - 2\theta$ X-ray diffraction (XRD) measurements. Three pronounced ZnO diffraction peaks, (1 0 0), (0 0 2) and (1 0 1) appear at $2\theta = 31.86°$, 34.68° and 36.46°, respectively, as shown in Fig. 1. The lattice constants calculated from the XRD pattern are $a = 3.240$ Å, $c = 5.167$ Å, and are very close to those of wurtzite ZnO, i.e., $a = 3.249$ Å, $c = 5.207$ Å [8]. This result indicates that ZnO has a polycrystalline hexagonal wurtzite structure with a preferred (0 0 2) orientation. In order to evaluate the average grain size of the films, the Scherrer's equation [9] is adopted. The average

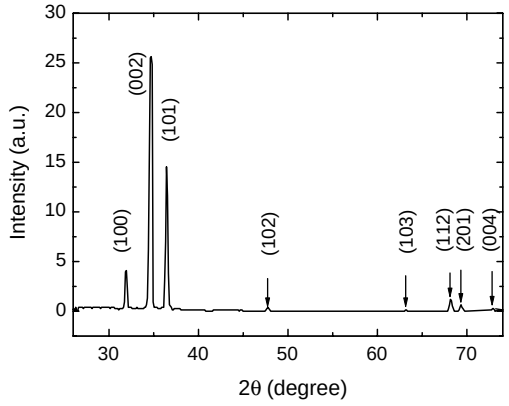

Fig. 1. XRD pattern of ZnO films annealed at a temperature of 800°C.

grain size for all the films annealed at 800°C is about 33 nm. Polycrystalline dimensions determined by atomic force microscopy (AFM) are in the 30–40 nm range. This value is consistent with the result of above XRD.

Fig. 2 shows the dependence of the PL spectra on temperature in the range 82–411 K; their main features of the PL spectra are similar. The luminescence spectra consist of the near-band-edge (NBE) emission and the deep-level (DL) emission. The inset of Fig. 2 shows an enlargement of the NBE emission at 82 K. It is remarkable that the DL emission band around 2.5 eV is barely observable. The intensity ratios of the NBE emission to the DL emission are 82 and 22 at 82 K and RT, respectively. At a low temperature of 82 K, both dominant emission lines in the spectrum can be attributed to free excitons and excitons bound to neutral acceptors, labeled as E_A and I_9 [8,10], respectively, as is discussed later. The line widths of the dominant excitonic emission lines at 3.35 and 3.31 eV for the spectrum at 82 K are as narrow as 28.9 and 27.0 meV, respectively. In general, the line width of the exciton emission at low-temperature PL is sensitive to local strain in the films. A narrow line width is a result of small residual strain. The low energy tail observed is due to the phonon replica of the bound exciton (I_9)

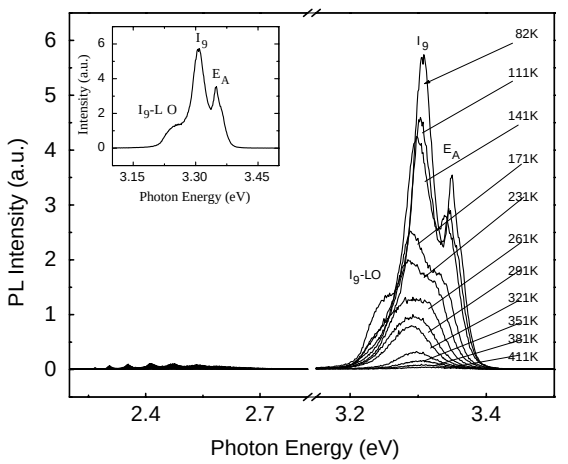

Fig. 2. PL measured at temperatures ranging from 82 to 411 K for ZnO films. The inset shows the enlargement of near-band-edge emission at 82 K.

[11,12]. The binding energy of the excitons bound to neutral acceptors I_9 is estimated to be 19.8 meV. This value agrees well with the reported value [10]. The temperature dependence of PL, as shown in Fig. 2, shows that the intensity of bound exciton emissions decreases rapidly from low to high temperature. The free exciton emission finally dominates the PL spectrum at about 230 K. The exciton emission is still clearly visible when the temperature increases to 411 K.

The peak position shifts to low energy when the temperature increases from 82 K to room temperature (RT). However, the peak positions undergo blueshifts and the full-width at half-maximum (FWHM) obviously broadens when the temperature increases from RT to 411 K. This is because the bound excitons are thermally ionized and the carriers may take part in PL at high-temperature. The PL intensity exponentially decreases in the higher-temperature region, mainly due to thermally activated nonradiative recombination mechanism. This luminescence quenching is characterized by relatively high activation energy.

The temperature dependence of the PL intensity can be expressed by the equation [13,14]

$$I(T) = I_0/[1 + A\exp(-E/k_B T)], \quad (1)$$

where E is the activation energy of the thermal quenching process, k_B is Boltzman constant, I_0 is the emission intensity at 0 K, T is a thermodynamic temperature and A is a constant. The solid line in Fig. 3 is the theoretical fit to the experimental data and we obtain $E = 60$ meV. This value is consistent with the exciton binding energy of 59 meV [1] in a bulk ZnO crystal. This result is evidence that the dominant emission peak (E_A) is from radiative recombination of free excitons. The peak positions as a function of temperature are shown in Fig. 4. A shift in the exciton energy results essentially from a band gap shift and thermally ionized bound excitons if it is assumed that exciton binding energy is temperature independent. As is well known, this derives from both thermal expansion and exciton–phonon interaction. The dependence of both mechanisms on temperature is very similar, and all phonons, in principle, contribute to the shift. The overall contribution to the shift can be determined by

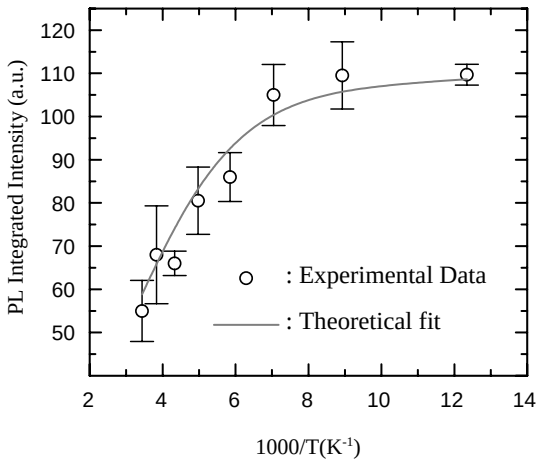

Fig. 3. The PL integrated intensities of peak E_A as a function of temperatures ranging from 82 to 290 K. The theoretical simulation (solid curve) to the experimental data points (○) is obtained using the equation $I = I_0/(1 + A\exp(-E/k_BT))$.

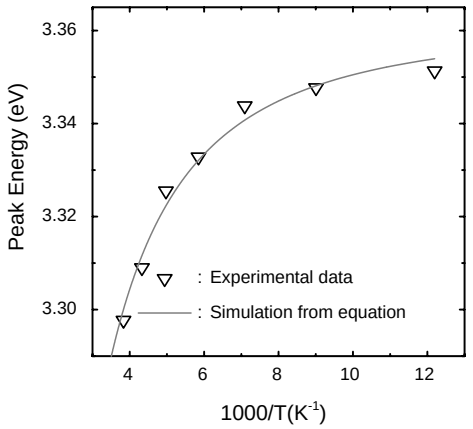

Fig. 4. Peak (E_A) energies as a function of temperature. Down triangles (▽) are experimental data, and the solid curve represents the fitting results based on the equation: $E(T) = E(0) - \lambda/[\exp(\omega\hbar/k_BT) - 1]$.

the Einstein approximation using the effective phonon energy $\varpi\hbar$. In this case, the variation of exciton energy with temperature is given by [7]

$$E(T) = E(0) - \lambda/[\exp(\omega\hbar/k_BT) - 1], \quad (2)$$

where $E(0)$ is an exciton energy at $T = 0$ K, and λ is a proportionality coefficient, $\varpi\hbar$ is the effective phonon energy. The solid curve in Fig. 4 is the theoretical fit to the experimental data for the nanocrystalline ZnO films. We obtain $E(0) = 3.37$ eV, $\lambda = 44.68$ meV and $\varpi\hbar = 11.44$ meV from the theoretical fitting. The fitted $\varpi\hbar$ (11.44 meV) approximately corresponds to the maximum energy of a low-frequency group of ZnO bulk phonons (12 meV). The λ obtained from the nanocrystalline ZnO thin films is larger than 20.9 meV, in Ref. [7]. This is because, for our calculation, λ is from the low-temperature emission spectra and the nanocrystalline ZnO films, while λ in the literature is from the low-temperature absorption spectra and the ZnO thin films.

Fig. 5 shows the dependence of FWHM on temperature, which could be interpreted as a broadening due to the exciton–phonon scattering. Thus, we did not consider the piezoelectric contribution because the exciton is an electrically neutral element excitation. The interaction between excitons and LO phonons is dominant at temperatures higher than 100 K. The experimental data for FWHM (Γ) could be simulated by the following theoretical formula [7,17,18]:

$$\Gamma(T) = \Gamma_0 + \gamma_{ph}T + \Gamma_{LO}/[\exp(\hbar\omega_{LO}/k_BT) - 1], \quad (3)$$

where $\hbar\omega_{LO}$ is a LO phonon energy, Γ_0 is the broadening parameter at 0 K, γ_{ph} is the coupling strength of an exciton–acoustic phonon interaction and Γ_{LO} is a parameter describing exciton–LO

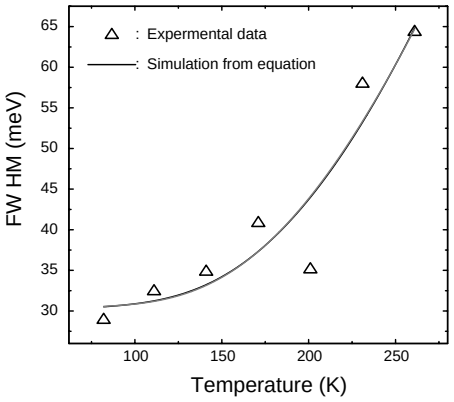

Fig. 5. The FWHM of the peaks (E_A) plotted against temperature. Up triangles (△) are the experimental data. The solid curve is the fitting result from the equation: $\Gamma(T) = \Gamma_0 + \gamma_{ph}T + \Gamma_{LO}/[\exp(\hbar\omega_{LO}/k_BT) - 1]$.

phonon interaction, T is thermodynamic temperature. A good fitting result is obtained as follows: $\hbar\omega_{LO} = 72\,\text{meV}$, $\gamma_{ph} = 10.8\,\mu\text{eV/K}$, $\Gamma_{LO} = 735\,\text{meV}$. The exciton–acoustic-phonon coupling strength (γ_{ph}) is similar to values reported for other semiconductors such as GaN, ZnSe [15,16]. However, the exciton–LO phonon coupling (Γ_{LO}) is smaller than 876.1 meV, in Ref. [7], while this value is larger than the results reported for GaN, ZnSe semiconductors [15,16]. First, this is because the polarity of ZnO is much larger than that of GaN, ZnSe semiconductors. Second, as is well known, the major process that contributes to exciton line width broadening is that a ground state (1S) exciton either dissociates into the free-electron-hole continuum or scatters within the discrete exciton bands by absorbing LO phonon via the high Fröhlich interaction [19]. Here, Γ_{LO} is dependent on the polarity of the materials and the quantum confinement effect. For bulk ZnO, the LO phonon energy is 72 meV [20]. Therefore, there must be many channels for exciton dissociation, which together with the high polarity, gives rise to rather large Γ_{LO} for ZnO. Because of the quantum confinement effect for the nanocystalline ZnO thin films, the energy separation between 1S and the first excited state (2S) becomes large, and the dissociation efficiency of 1S exciton into the first excited state (2S) or other excited states of the continuum states is largely suppressed. The transition from the ground state (1S) to other excited states including 2S state is reduced and Γ_{LO} is effectively reduced. This explains the further reduction of Γ_{LO} in our experiment.

4. Conclusions

The properties of the excitonic PL spectra, for nanocrystalline ZnO thin films prepared by thermal oxidation, are investigated in the temperature range from 82 to 411 K. A strong ultraviolet (UV) emission peak at 3.26 eV is observed, while the deep-level emission band is barely observable at room temperature. The UV emission is assigned to the free excitons. This study is consistent with the theoretical fitting. The strength of exciton–longitudinal-optical (LO) phonon coupling (Γ_{LO}) is deduced from the temperature dependence of the FWHM of the fundamental excitonic peak. The free exciton emissions are maintained at 411 K.

Acknowledgements

The authors would like to thank Dr. J. Judy for her helpful discussions. This work was supported by the Program of CAS Hundred Talents, the National Fundamental Applied Research Project, the Key Project of the National Natural Science Foundation of China No. 69896260, the National Natural Science Foundation of China, the Innovation Foundation of CIOFP, Excellent Young Teacher Foundation of Ministry of Education of China, and Jilin Distinguished Young Scholar Program.

References

[1] K. Hümmer, Phys. Stat. Sol. 56 (1973) 249.
[2] P. Yu, Z.K. Tang, G.K.L. Wong, M. Kawasaki, A. Ohtomo, H. Koinuma, Y. Segawa, Solid State Commun. 103 (1997) 459.
[3] D.M. Bagnall, Y.F. Chen, Z. Zhu, T. Yao, S. Koyama, M.Y. Shen, T. Goto, Appl. Phys. Lett. 70 (1997) 2230.
[4] H. Cao, Y.G. Zhao, H.C. Ong, S.T. Ho, J.Y. Dai, J.Y. Wu, R.P.H. Chang, Appl. Phys. Lett. 73 (1998) 3656.
[5] T. Makino, G. Isoya, Y. Segawa, C.H. Chia, T. Yasuda, M. Kawasaki, A. Ohtomo, K. Tamura, H. Koinuma, J. Cryst. Growth. 214/215 (2000) 289.
[6] R. Heitz, C. Fricke, A. Hoffmann, I. Broser, Mater. Sci. Forum 83–87 (1992) 1241.
[7] T. Makino, C.H. Chia, N.T. Tuan, Y. Segawa, M. Kawasaki, A. Ohtomo, K. Tamura, H. Koinuma, Appl. Phys. Lett. 76 (2000) 3549.
[8] Y. Chen, D.M. Bagnall, H.J. Koh, K.T. Park, K. Hiraga, Z.Q. Zhu, T. Yao, J. Appl. Phys. 84 (1998) 3912.
[9] B.D. Cullity, Elements of X-ray Diffractions, Addition-Wesley, Reading, MA, 1978, p. 102.
[10] J. Gutowski, N. Presser, I. Broser, Phys. Rev. B 38 (1988) 9746.
[11] Y. Chen, D.M. Bagnall, Z. Zhu, T. Sekiuchi, K.T. Park, K. Hiraga, T. Yao, S. Koyama, M.Y. Shen, T. Goto, J. Cryst. Growth. 181 (1997) 165.
[12] D.M. Bagnall, Y.F. Chen, M.Y. Shen, Z. Zhu, T. Goto, T. Yao, J. Cryst. Growth. 184/185 (1998) 605.
[13] P.O. Holtz, B. Monemar, H.J. Lozykowski, Phy. Rev. B 32 (1985) 986.

[14] D.S. Jiang, H. Jung, K. Ploog, J. Appl. Phys. 64 (1988) 1371.
[15] K.P. Korona, A. Wysmolek, K. Pakula, R. Stepniewski, J. Baranowski, I. Grzegory, B. Lucznik, M. Wrobleski, S. Porowski, Appl. Phys. Lett. 69 (1996) 7881.
[16] F. Bogani, L. Carraresi, A. Filoramo, S. Savasta, Phys. Rev. B 46 (1992) 9461.
[17] R. Hellmann, M. Koch, J. Feldmann, S.T. Lundiff, E.O. Gobel, D.R. Yakovler, A. Waag, G. Landwehr, Phys. Rev. B 48 (1993) 2847.
[18] M. O'Neill, M. Oestriech, W.W. Ruhle, D.E. Ashenford, Phys. Rev. B 48 (1993) 8980.
[19] N.T. Pelekanos, J. Dingm, M. Hagerott, A.V. Nurmikko, H. Luo, N. Samarth, J.K. Furdyna, Phys. Rev. B 45 (1992) 6037.
[20] E. Mollwo, In semiconductors: physics of II–VI and I–VII compounds, in: O. Madelung, M. Schulz, H. Weiss (Eds.), Semimagnetic Semiconductors, Landolt–Börnstein New Series, Vol. 17, Springer, Berlin, 1982, p. 35.